International Journal of Innovative
Computing, Information and Control
Volume **16**, Number **2**, April **2020**

ICIC International ©2020 ISSN 1349-4198
pp. **429–443**

INTEGRATION OF SOLAR TRACKER AND MAXIMUM POWER POINT TRACKING FOR IMPROVING PHOTOVOLTAIC (PV) SYSTEM EFFICIENCY

Aryuanto Soetedjo, Irrine Budi Sulistiawati and Yusuf Ismail Nakhoda

Department of Electrical Engineering
National Institute of Technology (ITN) Malang
Jalan Raya Karanglo KM 2, Malang 65143, Indonesia
aryuanto@gmail.com

Received July 2019; revised November 2019

Abstract. *This paper presents a method to integrate the solar tracker and the maximum power point tracking (MPPT) to improve the photovoltaic (PV) system efficiency. The integrated system provides a closed-loop solar tracker without the sensors. Instead of using the solar sensor, the output power of the MPPT is employed as the feedback signal to the solar tracker. The solar tracker estimates the solar azimuth and elevation angles using an astronomical algorithm based on the latitude, longitude and the date-time of the local site. To improve the solar tracking accuracy, the fuzzy logic controller is employed to adjust the angle according to the power slope of maximum power with respect to the solar tracker angle. From the simulation results, the proposed method increases the PV energy by 23.23% compared to the fixed PV panel. It improves the efficiency of the existing integrated solar tracker by 0.25% based on the simulation models.*
Keywords: Photovoltaic system, Solar tracker, Maximum power point tracking, Fuzzy logic, Solar position

1. **Introduction.** The most prominent factors that affect the efficiency of photovoltaic (PV) system are the solar incident angle and the nonlinear characteristic of the power and voltage (P-V) of the PV module. To maximize solar energy absorption due to the solar incident angle, the solar tracker system is utilized [1]. While to overcome the problem of nonlinear characteristic, the maximum power point tracking (MPPT) system is employed [2]. The first tracking system (solar tracker) is used to track the position of the solar by moving the PV panel so that the solar beam is perpendicular. While the MPPT adjusts the PV voltage to track the maximum power point of the PV when the solar irradiation changes.

Several advanced techniques on the solar tracker systems were proposed in [3-6]. In [3], the optical filter was installed on the solar sensor to reduce the noise caused by the diffused light. To correct the error of the model and the date, an adaptive controller was employed in [4]. The effect of spacing between PV arrays to the tracking efficiency was investigated in [5]. In [6], the heuristic approach was proposed to optimize the tracking accuracy and the energy consumption of the solar tracker system.

The importance of selecting a suitable MPPT technique was discussed in [7], where the work in [7] showed that the current-voltage characteristic at the maximum power point for the different PV modules has the different behavior. Since measuring both the solar irradiation and the temperature of the PV module requires the extra hardware, the MPPT technique proposed by [8] employed the adaptive Neuro-Fuzzy and the climatic

DOI: 10.24507/ijicic.16.02.429

estimator to estimate those parameters. The MPPT technique for the large PV system was proposed by [9], where the MPPT operated on each PV module independently. This approach increased PV efficiency.

The most popular MPPT techniques are the Perturb and Observe (P&O) method [10,11], the Incremental Conductance method [12], and the Fuzzy method [13]. The P&O method finds the maximum power point by perturbing the voltage and observing the resulted power to govern the direction of voltage perturbation in the next cycle. The Incremental Conductance method is based on the fact that the gradient of the P-V curve is zero at the maximum point, positive at the left side and negative at the right side of the maximum power point. Using simple mathematics, it could be obtained that the maximum condition is achieved when the incremental conductance is the same as the instantaneous conductance. Thus the incremental conductance method works by comparing the incremental conductance and the instantaneous conductance. The fuzzy-based MPPT [13] employed the fuzzy system to adjust the perturbation step size of the P&O method to increase the tracking speed while minimizing the oscillation at the maximum power point.

In general, the solar tracking system is divided into sensor-based solar tracker [14-16] and sensorless solar tracker [17-19]. The sensor-based solar tracker uses the light dependent resistor (LDR) sensors or photodiode sensors to sense the maximum solar irradiance that falls into the PV panel. Typically, the sensor-based solar tracker uses two sensors [14], four sensors [15], and five sensors [16]. In the sensorless solar tracker system, the solar position is expressed in the terms of the solar azimuth and the solar elevation. Mathematically, the solar azimuth and the solar elevation could be derived from the geographic latitude and longitude of PV location, and the date and the universal time. In [17], a global position system (GPS) and a personal computer (PC) were used to calculate the solar azimuth and elevation angles for thirty days based on the solar position algorithm (SPA) [18]. In [19], the Astronomical Almanac's (AA) [20] was used for calculating the solar position. To provide robust tracking, optimal control was proposed in [21] for minimizing the error between the solar elevation angle and the actual PV panel elevation angle.

The sensor-based solar tracker is a closed-loop system which provides high accuracy. However, it has several drawbacks, such as a) it requires a complicated sensor installation, and b) it could not track the solar in the cloudy condition. While the sensorless solar tracker is an open loop system which is simple in the hardware implementation and it is able to track the solar during the cloudy condition. However, since the solar position is calculated mathematically, the accuracy is lower due to the estimated value rather than the real one. One way to increase the tracking performance is by employing the hybrid solar tracker which combines the sensor-based and sensorless tracker as proposed in [22,23]. In the hybrid solar tracker, at first, the solar azimuth and elevation angles are calculated to rotate the tracker. Then the tracker is tuned using the information from the LDR sensors. Moreover, the hybrid approach provides an additional function as a redundancy system, i.e., the tracker still works when the sensors fail and vice versa [23].

The impacts of the MPPT and the solar tracker were investigated in [24], where the authors compared three methods, i.e., without MPPT and without solar tracker, with MPPT and without solar tracker, and with MPPT and with solar tracker. The results showed that compared to the first method, the second and the third methods increase the PV power 18% and 100% respectively.

The other interesting approaches are by integrating the MPPT and the solar tracker as proposed in [25,26]. Instead of controlling the MPPT and the solar tracker independently [24], the approaches [25,26] combined both techniques concurrently, in the sense that the

output of MPPT system was used to control the solar tracker. In [25], four light sensors were employed as solar sensor of the dual-axis solar tracker. The azimuth and elevation angles of the tracker are adjusted by a fuzzy logic controller (FLC) whose inputs are the change of power generated by MPPT and the error of current of the sensors. In [26], initially the sensorless solar tracker rotated the PV panel to follow the azimuth and elevation angles based-on the geographic location. Then the azimuth and elevation angles were increased or decreased according to the slope of maximum power, which is defined as the change of the maximum power generated by the MPPT divided by the change of the azimuth or elevation angle.

The methods of existing works are summarized in Table 1. As shown in the table, several efforts are proposed to improve PV efficiency by the combination techniques such as the hybrid sensor-based and sensorless sensor tracker, and the combination of MPPT and solar tracker. As reported by [24], the combination of MPPT and the solar tracker improves the PV efficiency significantly. However, since they work independently, the solar tracker does not have the information whether the tracked position achieves the maximum power of the PV which is obtained by the MPPT method. Thus it suggests utilizing the output of the MPPT to control the solar tracker as proposed in [25,26]. Compared to [25], the work in [26] provides an efficient method, since it does not require the sensor installation.

Table 1. The methods of existing works

Method			**Reference**
MPPT			[2,8-13]
Solar tracker	Sensor-based		[14-16]
	Sensorless		[17,19]
	Hybrid sensor-based and sensorless		[22,23]
Combination of MPPT and solar tracker	Work independently		[24]
	Work concurrently	MPPT + Sensor-based solar tracker	[25]
		MPPT + Sensorless solar tracker	[26]

In this paper, we propose a method to improve the work in [26] by employing the FLC to adjust the azimuth and elevation angles of the solar tracker. Instead of using a fixed step angle, our method uses a variable step angle determined by the FLC. By introducing the FLC and the variable step angle, the tracker performance could be improved. Moreover, to increase the accuracy and the tracking speed, the DC motor is used instead of the stepper motor.

The rest of paper is organized as follows. Section 2 describes our proposed system. The simulation results are discussed in Section 3. Finally, the conclusion is covered in Section 4.

2. **Proposed System.**

2.1. **System description.**

2.1.1. *Architecture of the system.* The architecture of the proposed system is illustrated in Figure 1. The upper part is the sensorless solar tracker, while the lower part is the MPPT. The solar tracker system consists of the solar azimuth and elevation angles calculator, the solar tracker controller, the DC motors, the PV panel, and the supporting platform. The solar azimuth and elevation angles calculator is used to calculate the solar position based-on the local geographic latitude, longitude, the date and the time. Then the resulted

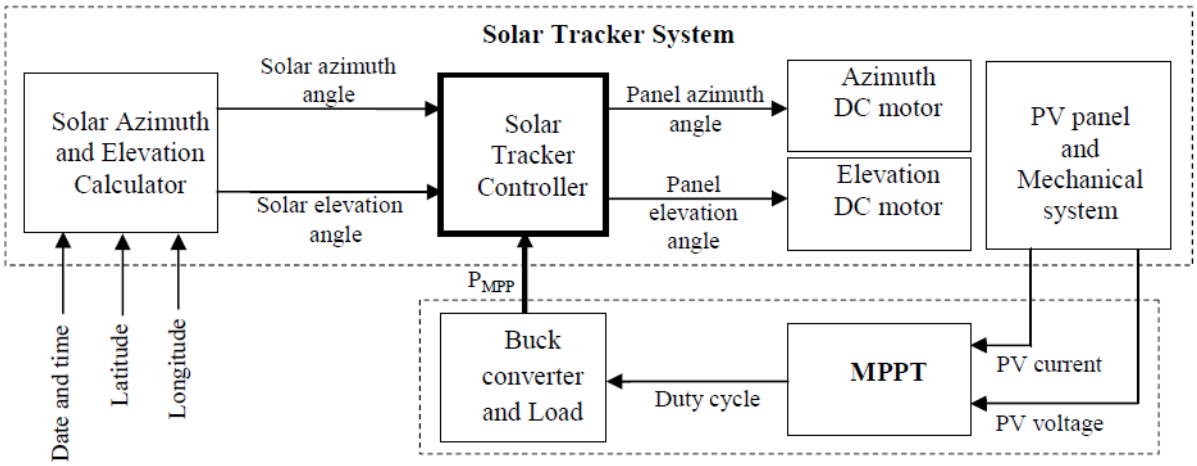

FIGURE 1. Architecture of proposed system

solar azimuth and elevation angles are used by the solar tracker controller to rotate the PV panel to the proper position, i.e., the PV panel surface is perpendicular to the solar beam. The DC motors are used to rotate the supporting platform of the PV panel.

The MPPT controls the duty cycle of the DC-DC converter (buck converter) to achieve the maximum power using the popular P&O algorithm. According to [26], the maximum power could be employed as the feedback signal to adjust the azimuth and elevation angles of the PV panel as described in the following. Let $P_{MPP}(k+1)$, $\alpha(k+1)$, $\gamma(k+1)$ be the maximum power, the PV panel azimuth angle, the PV panel elevation angle at $(k+1)^{\text{th}}$ step respectively, $P_{MPP}(k)$, $\alpha(k)$, $\gamma(k)$ be the maximum power, the PV panel azimuth angle, the PV panel elevation angle at $(k)^{\text{th}}$ step respectively. The power slopes $M\alpha$ and $M\gamma$ are expressed as

$$M\alpha = \frac{P_{MPP}(k+1) - P_{MPP}(k)}{\alpha(k+1) - \alpha(k)} \tag{1}$$

$$M\gamma = \frac{P_{MPP}(k+1) - P_{MPP}(k)}{\gamma(k+1) - \gamma(k)} \tag{2}$$

Then the solar tracker is in the proper position, i.e., yields the maximum power, when both $M\alpha$ and $M\gamma$ are zero.

The control strategy to achieve the maximum power is by adjusting the PV panel azimuth and elevation angles with the variable step angles, which are determined by the FLC as described in the next section.

2.1.2. *Fuzzy logic controller of solar tracker.* The configuration of FLC to control the solar tracker is illustrated in Figure 2. As shown in the figure, each solar azimuth tracker and solar elevation tracker is controlled by the FLC called as FLC-Solar Azimuth Tracker (FLC-AT) and FLC-Solar Elevation Tracker (FLC-ET). The output of FLC-AT is the azimuth step angle ($\Delta\alpha$), which is used to increase or decrease the azimuth angle α. The inputs of FLC-AT are the power slope $M\alpha$ which is defined by (1), and the change of power slope ($\Delta M\alpha$) which is defined as

$$\Delta M\alpha = M\alpha(k+1) - M\alpha(k) \tag{3}$$

where $M\alpha(k+1)$ and $M\alpha(k)$ are the power slope $M\alpha$ at $(k+1)^{\text{th}}$ step and $(k)^{\text{th}}$ step respectively. The output of FLC-ET is the elevation step angle ($\Delta\gamma$), which is used to increase or decrease the elevation angle γ. The inputs of FLC-ET are the power slope

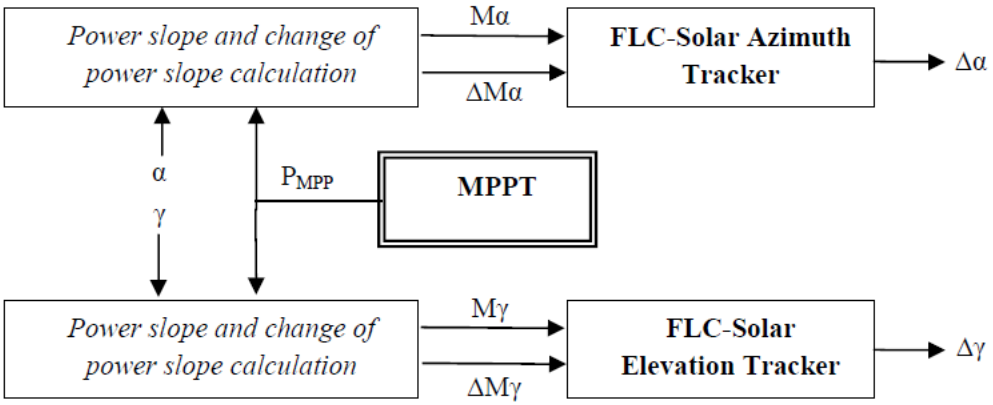

FIGURE 2. Configuration of FLC solar tracker

$M\gamma$ which is defined by (2), and the change of power slope ($\Delta M\gamma$) which is defined as

$$\Delta M\gamma = M\gamma(k+1) - M\gamma(k) \tag{4}$$

where $M\gamma(k+1)$ and $M\gamma(k)$ are the power slope $M\gamma$ at $(k+1)^{\text{th}}$ step and $(k)^{\text{th}}$ step respectively.

Both the FLC-AT and the FLC-ET have a similar configuration. Therefore, only the FLC-AT will be discussed in the following. As shown in Figure 2, the objective of the FLC-AT is to adjust the azimuth step angle based-on the power slope and its derivative. This task could be accomplished intuitively using the fuzzy rules. Therefore, the fuzzy Mamdani inference system is adopted since its fuzzy rules are easy to be understood, more intuitive, and suited for the human expert.

The input variables $M\alpha$ and $\Delta M\alpha$, and the output variable $\Delta\alpha$ have five linguistic values, i.e., Negative Big (NB), Negative Small (NS), Zero (ZE), Positive Small (PS), Positive Big (PB), where their membership functions are illustrated in Figure 3. As shown in the figure, the ranges of variables are normalized into -1 to 1 for simplifying the tuning process.

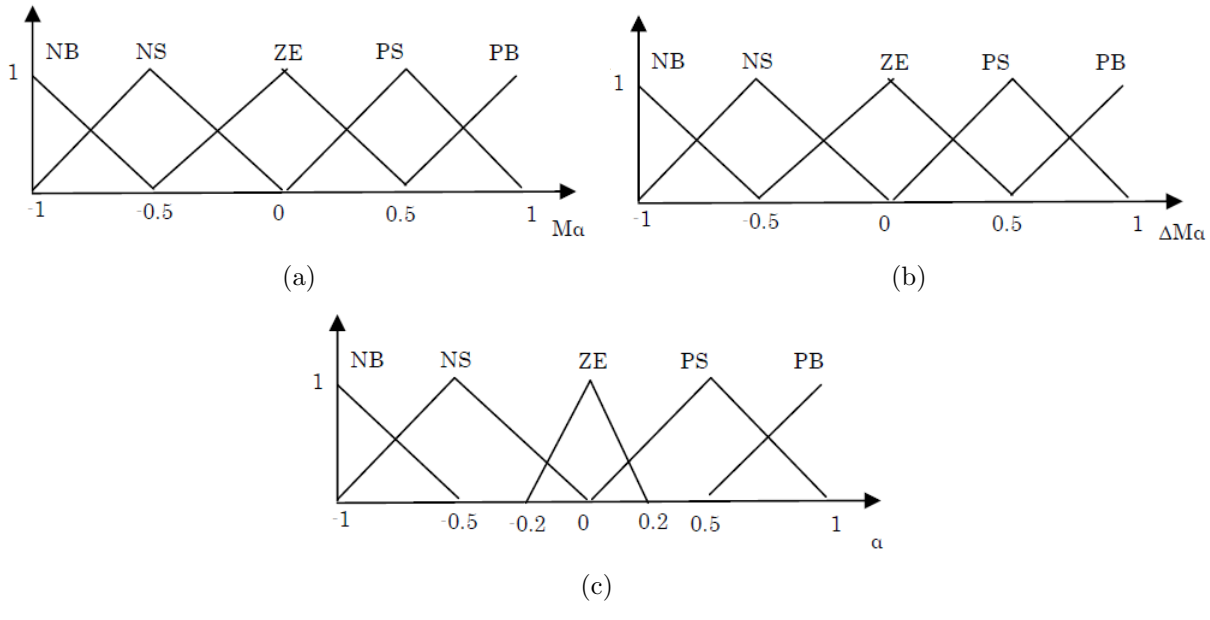

FIGURE 3. Membership functions of: (a) $M\alpha$; (b) $\Delta M\alpha$; (c) α

The fuzzy rules are given in Table 2, which are defined based on the characteristics of the power slope in conjunction with the maximum power such as:

- IF $M\alpha$ is Negative Big (NB) AND $\Delta M\alpha$ is Zero (ZE), THEN $\Delta\alpha$ is Negative Big (NB): That the power slope is negative big and the change of power slope is zero means that the operating point of the tracker is located far away in the right side of the maximum point. Thus it suggests that the azimuth angle should be reduced largely, i.e., step angle is negative big.
- IF $M\alpha$ is Positive Small (PS) AND $\Delta M\alpha$ is Zero (ZE), THEN $\Delta\alpha$ is Positive Small (PS): That the power slope is positive small and the change of power slope is zero means that the operating point of the tracker is located in the left side and near to the maximum point. Thus it suggests that the azimuth angle should be increased slightly, i.e., step angle is positive small.
- IF $M\alpha$ is Zero (ZE) AND $\Delta M\alpha$ is Zero (ZE), THEN $\Delta\alpha$ is Zero (ZE): It is the condition at the maximum point, thus the azimuth angle should not be changed, i.e., step angle is zero.

Table 2. Fuzzy rules of FLC-AT

	$\boldsymbol{\Delta M\alpha}$				
$\boldsymbol{M\alpha}$	**NB**	**NS**	**ZE**	**PS**	**PB**
NB	ZE	ZE	NB	NB	NB
NS	ZE	ZE	NS	NS	NS
ZE	NS	ZE	ZE	ZE	PS
PS	PS	PS	PS	ZE	ZE
PB	PB	PB	PB	ZE	ZE

2.2. **System modeling.**

2.2.1. *Integrated solar tracker and MPPT modeling.* The proposed integrated solar tracker and MPPT is modeled as illustrated in Figure 4. The system consists of the PV azimuth angle control system model, the PV elevation angle control system model, the PV model, the MPPT model, the FLC-AT model, the FLC-ET model, the solar position algorithm, and the effective solar irradiation calculation.

Our proposed system improves the existing approach [26] in twofold. First, our approach employs the FLC to control the step angles of the solar tracker. The FLC provides the variable step values to control the azimuth and elevation angles of the solar tracker system. Meanwhile, the approach in [26] controls those angles using the fixed step values, which are determined by nine rules according to the values of power slopes. Second, instead of using the stepper motor systems [26] with the resolutions of 0.12°, our approach uses the DC motors that offer a smaller resolution (continuous rotation). By using the variable step angles and the DC motors, the azimuth and elevation angles could be controlled more accurately. Moreover, the FLC technique offers better tracking performance.

It is important to note that since the proposed system is a simulation model, two problems occur, i.e.: a) the problem of simulating the effective irradiation due to the tilt and azimuth angles of PV panel, b) the problem of simulating the inaccuracy of the solar position generated by the solar position algorithm. The first problem is solved by introducing the effective solar irradiation calculation as described in the following section. The second problem is solved by introducing the disturbing angle as shown in the top part of Figure 4. Referring to the figure, there are two types of solar position: a) the

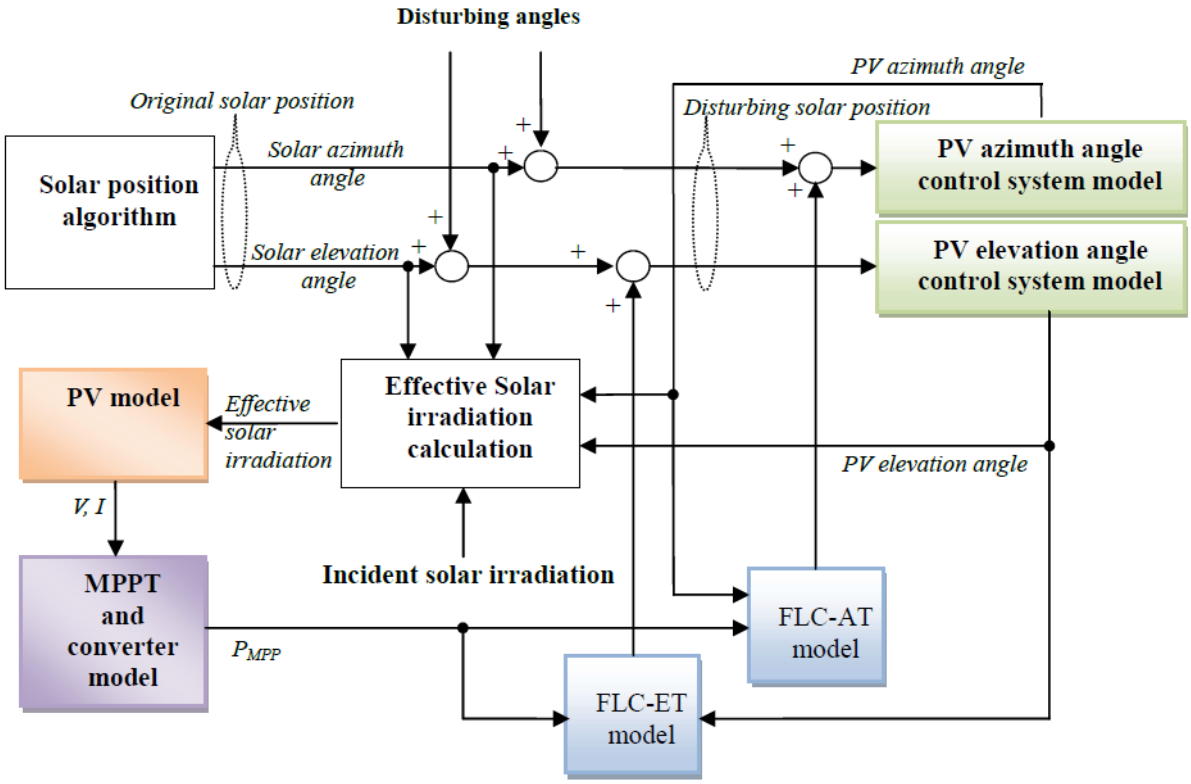

FIGURE 4. Integrated solar tracker and MPPT model

solar position generated by the solar position algorithm, which is called as the original solar position, b) the disturbing solar position, which is obtained by adding the disturbing angle to the original solar position. The original solar position is fed to the solar panel via the effective solar irradiation calculation. While the disturbing solar position is fed to the solar tracker directly. By this arrangement, we may examine the effectiveness of our method in solving the problem of the inaccuracy of the sensorless solar tracker.

2.2.2. *Solar position algorithm and effective irradiation calculation.* There are several methods to calculate the solar position such as Astronomical Almanac's (AA) [20], P-SA [27], SPA [18]. Our method employs the solar position algorithm proposed in [28-30] which is written in Matlab software by [31]. The algorithm is described as follows.

(a) Compute the day number (d), i.e., the number of days since J2000 (Julian calendar), as

$$d = JD - 2451543.5 \tag{5}$$

where JD is Julian day number, i.e., the number of days since January 1, 4713 BC.

(b) Compute the longitude of perihelion (w), i.e., the longitude of a point nearest to the sun in the orbit of the planet/earth

$$w = 282.9404 + 0.0000470935d \tag{6}$$

(c) Compute the orbital eccentricity (e)

$$e = 0.016709 - 0.000000001151d \tag{7}$$

(d) Compute the mean anomaly (M), i.e., the angle of fictitious planet that moving on a circle of the orbit with the same period as the real planet/earth that measured

from the perihelion

$$M = 356.0470 + 0.9856002585d \tag{8}$$

(e) Compute the solar's mean longitude (L), i.e., the longitude when the orbital is a perfect circle

$$L = w + M \tag{9}$$

(f) Compute the obliquity ($oblecl$), i.e., the angle between the ecliptic and the planes of the equator

$$oblecl = 23.4393 - 0.0000003563d \tag{10}$$

(g) Compute the Eccentric anomaly (E), i.e., the angle between the perihelion and the projection point of the planet/earth at the circular orbit that is measured on the center of the orbit

$$E = M + ((180/\pi)\sin(M(\pi/180)e)(1 + \cos(M(\pi/180))e)) \tag{11}$$

(h) Compute the rectangular coordinates in the plane of the ecliptic (x and y)

$$x = \cos(E(\pi/180)) - e \tag{12}$$

$$y = \sin(E(\pi/180))\left(1 - e^2\right)^{-2} \tag{13}$$

(i) Compute the distance between the solar and the earth (r), and true anomaly (v), i.e., the angle between the perihelion and the planet/earth that is measured on the center of the solar

$$r = \left(x^2 + y^2\right)^{-2} \tag{14}$$

$$v = \tan^{-1}(y/x)(180/\pi) \tag{15}$$

(j) Compute the longitude of the solar (lon)

$$lon = v + w \tag{16}$$

(k) Compute the ecliptic rectangular coordinates

$$xeclip = \cos(lon(\pi/180))r \tag{17}$$

$$yeclip = \sin(lon(\pi/180))r \tag{18}$$

$$zeclip = 0.0 \tag{19}$$

(l) Compute the equatorial rectangular coordinates

$$xequat = xeclip \tag{20}$$

$$yequat = (yeclip\cos(oblecl(\pi/180))) + (zeclip\sin(oblecl(\pi/180))) \tag{21}$$

$$zequat = (yeclip\sin(23.4406(\pi/180))) + (zeclip\cos(oblecl(\pi/180))) \tag{22}$$

(m) Compute the right ascension (RA), i.e., the angular location along the celestial equator (longitude) and declination ($Decl$), i.e., the distance from the celestial equator (latitude)

$$rr = \left(xequat^2 + yequat^2 + zequat^2\right)^{-2} - (Alt/149598000) \tag{23}$$

$$RA = \tan^{-1}(yequat/xequat)(180/\pi) \tag{24}$$

$$Decl = \sin^{-1}(zequat/rr)(180/\pi) \tag{25}$$

where Alt is the altitude of the local site above the sea.

(n) Compute the local sidereal time ($SIDTIME$), i.e., the coordinate of the RA on the observer's meredian

$$GMST0 = (L + 180)/15 \tag{26}$$
$$SIDTIME = GMST0 + UTH + Longi/15 \tag{27}$$

where $GMST0$ is the Greenwich Mean Sidereal Time at 00:00 Universal time, UTH is Greenwich time, $Longi$ is the longitude of the local site.

(o) Convert RA to hour angle (HA)

$$HA = (15SIDTIME - RA) \tag{28}$$

(p) Convert HA to the rectangular coordinate system (xc, yc, zc)

$$xc = \cos(HA(\pi/180))\cos(Decl(\pi/180)) \tag{29}$$
$$yc = \sin(HA(\pi/180))\cos(Decl(\pi/180)) \tag{30}$$
$$zc = \sin(Decl(\pi/180)) \tag{31}$$

(q) Rotate xc, yc, zc system along an axis going East-West

$$xhor = (xc\cos((90 - Lat)(\pi/180))) - (zc\sin((90 - Lat)(\pi/180))) \tag{32}$$
$$yhor = yc \tag{33}$$
$$zhor = (xc\sin((90 - Lat)(\pi/180))) + (z\cos((90 - Lat)(\pi/180))) \tag{34}$$

where Lat is the latitude of local site.

(r) Compute the solar azimuth (Az) and solar elevation (El)

$$Az = \tan^{-1}(yhor/xhor)(180/\pi) + 180 \tag{35}$$
$$El = \sin^{-1}(zhor)(180/\pi) \tag{36}$$

The solar energy absorbed by the PV panel will be maximum when the solar beam is perpendicular to the PV panel surface. To compute the effective solar irradiation when the PV panel surface is not perpendicular to the solar beam, the formula below is adopted.

$$Seff = Sind(\cos(\gamma)\sin(\beta)\cos(\theta - \alpha) + \sin(\gamma)\cos(\beta)) \tag{37}$$

where

$Seff$ = Effective solar irradiation,
$Sind$ = Incident solar irradiation,
α = Solar azimuth angle,
γ = Solar elevation angle,
θ = PV panel azimuth angle,
β = PV panel tilt angle.

2.2.3. *Solar tracker modeling.* The solar tracker consists of the FLC-AT, FLC-ET, PV azimuth angle control system and PV elevation angle control system. Both the PV azimuth and elevation angles control systems have the same model as illustrated in Figure 5. The model is the DC motor position control system using a PID controller, where K_p is the proportional gain, K_I is the integral gain, K_d is the differential gain, k_e is the motor constant, L_a is the armature inductance, f is the damping coefficient, R_a is the armature resistance, and J is the moment of inertia.

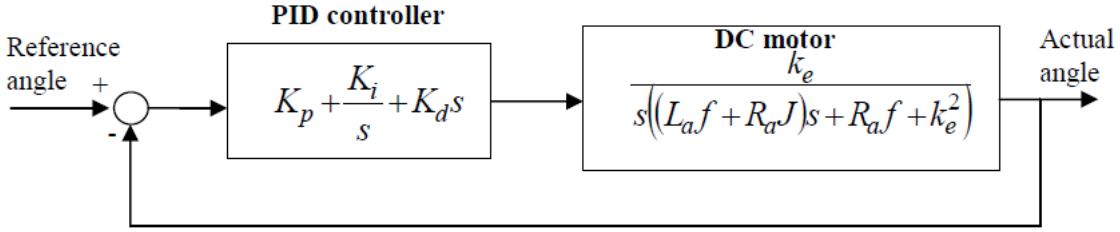

FIGURE 5. PID controller and DC motor model

2.2.4. *PV and buck converter modeling.* The PV model is adopted from [10,33], which is expressed by (38)-(41). The current-voltage characteristic of the PV is expressed as

$$I = I_L - I_0 \left(e^{\frac{q(V+IR_S)}{1.2kT}} - 1 \right) \tag{38}$$

where I and V are the PV current and voltage respectively, I_L is the photo current, I_0 is the saturation current of the diode, q is the charge on an electron (1.60×10^{-19} C), R_S is the series resistance, k is the Boltzman's constant (1.38×10^{-23} J/K), T is the working temperature. The photo current (I_L) is expressed as

$$I_L = I_{L(T_1)} \left(1 + \left(\frac{I_{SC(T_2)} - I_{SC(T_1)}}{T_2 - T_1} \right) (T - T_1) \right) \tag{39}$$

where $I_{L(T_1)}$ and $I_{SC(T_1)}$ are the photo current and the short circuit current at the temperature $T_1 = 25°$C respectively, $I_{SC(T_2)}$ is the circuit current at the temperature $T_2 = 75°$C. The saturation current of the diode (I_0) is expressed as

$$I_0 = \left(\frac{I_{SC(T_1)}}{e^{\frac{qV_{OC(T_1)}}{1.2kT_1}} - 1} \right) \left(\frac{T}{T_1} \right)^{2.5} \left(e^{\frac{-1.12q}{1.2k\left(\frac{1}{T} - \frac{1}{T_1}\right)}} \right) \tag{40}$$

where $V_{OC(T_1)}$ is the open circuit voltage at the temperature T_1. The series resistance (R_S) is calculated from

$$R_S = 0.0158 - \frac{1}{\left(\frac{I_{SC(T_1)}}{e^{\frac{qV_{OC(T_1)}}{1.2kT_1}} - 1} \right) \left(\frac{q}{1.2kT_1} \right) e^{\frac{qV_{OC(T_1)}}{1.2kT_1}}} \tag{41}$$

The buck converter model is adopted from [10,34], which is expressed by (42)-(45). The average inductor voltage (v_L) is expressed as

$$v_L = Dv_g - v_C - i_L \left(R_{ON} + R_L + ESR \right) + \left(i_{Load} ESR \right) \tag{42}$$

where D is the duty cycle, v_g is the input voltage, v_C is the capacitor voltage, i_L is the inductor current, R_{ON} is the resistance of the switching device at the ON state, R_L is the inductor resistance, ESR is the equivalent series resistance of the capacitor, i_{Load} is the load current (output current). The average capacitor current (i_C) is expressed as

$$i_C = i_L - i_{Load} \tag{43}$$

The output voltage (v_{Out}) is expressed as

$$v_{Out} = v_C + i_L ESR - i_{Load} ESR \tag{44}$$

The input current (i_g) is expressed as

$$i_g = i_L D + t_r i_L f_s + Q_r f_s \tag{45}$$

where t_r is the diode reverse recovery time, f_s is the switching frequency, and Q_r is the diode recovered charge.

3. **Simulation Results.** The proposed system is simulated using the Matlab-Simulink. To examine the effectiveness of our method, we compare five methods: a) Fixed panel: there is no solar tracker (**NTR**); b) Solar tracker using stepper motor proposed by [26] (**EXT**), where the stepper motor model in [35] is used; c) Solar tracker using DC motor without angle adjustment (**DCN**); d) Solar tracker using DC motor with fixed angle adjustment (**DCAJ**); e) Our proposed method, i.e., the solar tracker using DC motor with variable angle adjustment (**PROP**). The methods are simulated based on the PV module located at Malang city, Indonesia, longitude = 112.6326° E, latitude = 7.9666° S, and the date is April 20, 2019. The profile of solar irradiation from the time of 5 h to 18 h shown in Figure 6 is used to evaluate the methods.

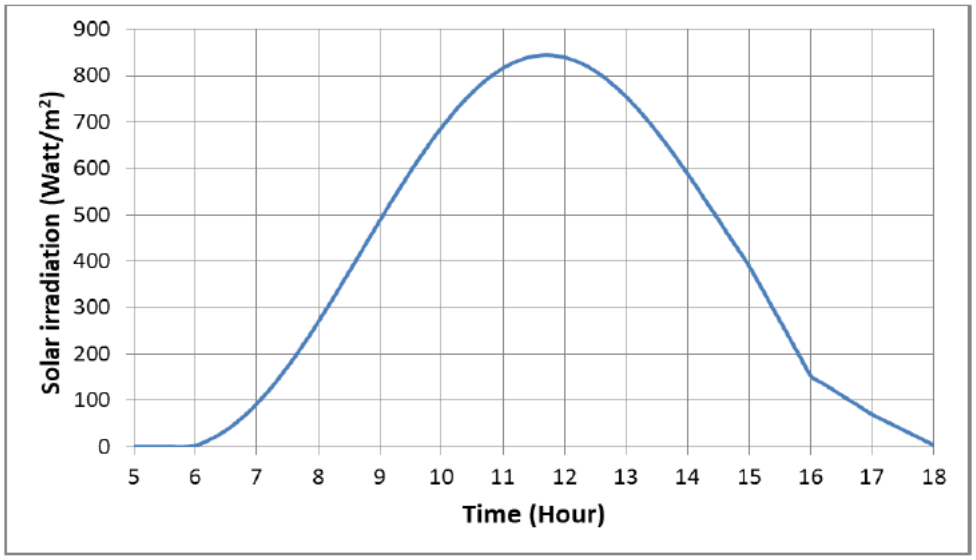

FIGURE 6. Profiles of solar irradiation

The parameters of PID controller are $K_p = 403.20$, $K_i = 1174.69$, $K_d = 10.12$. The DC motor used in the simulation is modelled by a transfer function as proposed in [32], where the motor constant $(k_e) = 0.99$, the armature inductance $(L_a) = 0.008$ H, the damping coefficient $(f) = 0.004$ Nms/rad, the armature resistance $(R_a) = 1.23\ \Omega$, and the moment of inertia $(J) = 0.021$ kgm^2. The electrical characteristics of the PV [10] are the maximum power $(P_{\max}) = 50$ W, the voltage at maximum power $(V_{mp}) = 17.5$ V, the current at maximum power $(I_{mp}) = 2.86$ A, the open circuit voltage $(V_{OC}) = 21.5$ V, and the short circuit current $(I_{sc}) = 3.25$ A. In the simulation, six PV modules are connected in parallel, thus the total power is 300 W. The parameters of the buck converter are the inductor inductance = 100 μH, the capacitor capacitance = 50 μF, $R_{ON} = 0.05\ \Omega$, $R_L = 0.1\ \Omega$, $ESR = 0.05\ \Omega$, $t_r = 50 \times 10^{-9}$ s, $f_s = 40$ kHz, $Q_r = 100 \times 10^{-9}$ C.

In the simulation, the PV energy from 5h to 18h is calculated to compare the effectiveness of the methods. Since the effectiveness of MPPT using P&O method is affected by the perturbation step size (ΔMPPT), this parameter is also considered in the comparison. The comparison results are given in Table 3. In the **NTR**, the PV panel azimuth and elevation angles are set to 30° and 60° respectively. In the **EXT**, the angle adjustment (ΔAdj) values of 0.12° (original method of [26]), 0.9° and 1.8° are evaluated. In the **DCAJ**, the angle adjustment (ΔAdj) values are 0.25°, 0.5° and 0.75°.

From the table, we may evaluate some results and findings as discussed in the following. The highest PV energy is achieved by our proposed method (**PROP**) (96955.353 W.min), the second and third highest are the **DCAJ** (96857.613 W.min) and **EXT** (96823.665

TABLE 3. Comparison of the simulation results

Method		PV energy (Watt minutes: W.min)			
		ΔMPPT = 0.1	**ΔMPPT = 0.2**	**ΔMPPT = 0.3**	**Maximum value**
NTR		78689.173	78677.525	78261.041	78689.173
EXT	Stepper angle = 0.12° ΔAdj = 0.12°	88332.767	96761.667	96404.442	96823.665
	Stepper angle = 0.9° ΔAdj = 0.9°	88408.175	96823.665	96447.312	
	Stepper angle = 1.8° ΔAdj = 1.8°	95961.885	96428.467	95961.885	
DCN		96660.954	96714.880	96444.404	96714.880
DCAJ	ΔAdj = 0.25°	96742.059	96814.794	96519.773	96857.613
	ΔAdj = 0.5°	96785.236	96857.613	96596.376	
	ΔAdj = 0.75°	96763.297	88414.772	96478.508	
PROP		96912.362	96955.353	96523.066	96955.353

W.min) respectively. This result shows that the efficiency of **DCAJ**, i.e., using DC motor with a fixed angle adjustment, is better than the existing method (**EXT**) that employs the fixed angle adjustment but using the stepper motor. It means that the tracking accuracy could be improved by using the DC motor instead of the stepper motor. Moreover, our proposed method (**PROP**) that employs the DC motor and introducing the variable angle adjustment generated by the FLC, achieves the highest efficiency.

By observing Table 3, we may examine that each method generally achieves the maximum PV energy when the value of ΔMPPT is 0.02. It conforms to the fact that a smaller perturbation step size reduces the MPPT's response time, while a bigger perturbation step size increases oscillation at the steady state. Both cases will reduce PV power. The similar phenomenon occurs in the ΔAdj for **EXT** and **DCAJ**, i.e., the variation of ΔAdj value changes the PV power and an optimal ΔAdj exists, which produces the maximum power. The optimum values of ΔAdj are 0.9° and 0.5° for the **EXT** and **DCAJ** respectively. These results show that selecting the values of ΔAdj and ΔMPPT is an important task in **EXT** and **DCAJ** methods since it affects the results significantly. In other words, we can say that finding the optimal values of those variables are very crucial in the existing techniques. However, our proposed method finds the optimal ΔAdj using the FLC technique. It is worth noting that in our proposed method, the selection of the values of ΔMPPT does not affect the result significantly.

Figure 7 shows the effective solar irradiation on the fixed PV panel and the solar tracker PV panel, where the solid line represents the incident solar irradiation, the dotted line represents the effective solar irradiation on a fixed panel (**NTR** method), and the dashed line represents the effective solar irradiation on a solar tracker (**PROP** method). It is clearly shown that the effective solar irradiation on the fixed panel (**NTR**) could not follow the incident solar irradiation, thus the generated PV power is low as given in Table 3. Meanwhile since the solar tracker (**PROP**) tracks the solar position, the effective solar irradiation is able to follow the incident solar irradiation, even though introducing a small deviation. Fortunately, this small deviation shows that the proposed model, i.e., by introducing the disturbing angles as shown in Figure 4, could be used to evaluate the effectiveness of the solar tracker system on handling the inaccuracy problem.

The PV energy which is generated by our proposed method (**PROP**) is 0.25% higher compared to the existing technique [26] (**EXT**). This small improvement is caused by the limitation of the model as described in the following. From Table 3, it is obtained that compared to the **NTR**, the PV energies which are generated by **EXT**, **DCN**, **DCAJ**,

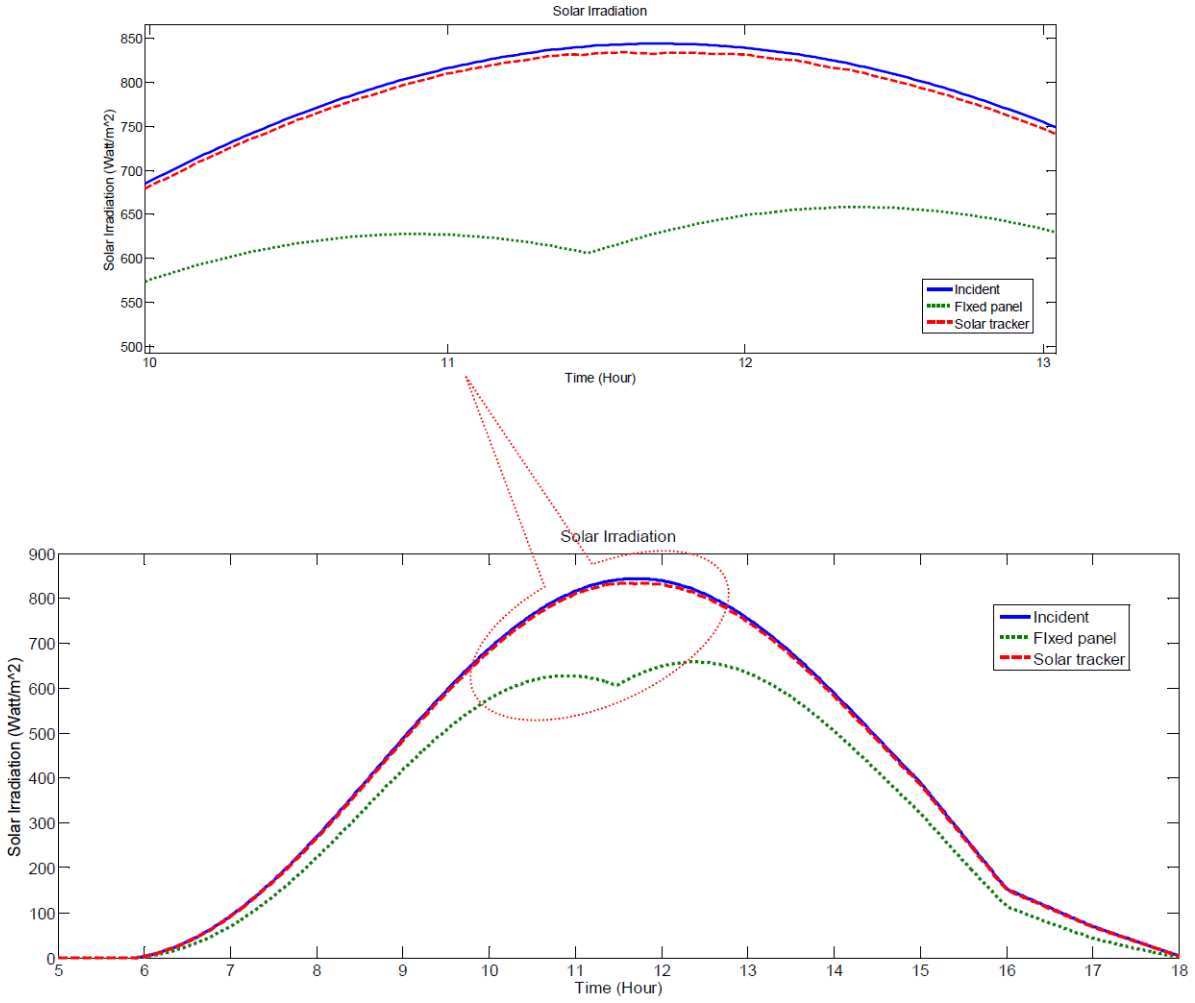

FIGURE 7. Effective solar irradiation

and **PROP** increase 22.98%, 22.92%, 23.09%, 23.23% respectively. The results show that the improvement achieved by **DCAJ** (a method similar to **EXT** but using the DC motor) is almost the same as the conventional solar tracker (**DCN**). Meanwhile, the author in [26] verifies by the hardware experiment that **EXT** improves the energy efficiency about 10% compared to the conventional solar tracker. It indicates that the PV and solar tracker models used here have a limitation for comparing the integrated solar tracker to the conventional solar tracker. This limitation is caused by the simplified models used in the simulation, such as the solar position modeling, the MPPT modeling, and the solar tracker system modeling. However, by comparing the results in Table 3 and the results obtained by [26], it suggests that our proposed method offers a promising method to improve the efficiency of the PV system by integrating the MPPT and the solar tracker system using the FLC.

4. **Conclusions.** Integration of the sensorless solar tracker and the MPPT is presented. The method takes advantage of the simple installation of the sensorless system. However, to improve the solar tracking accuracy, the FLC is employed for tuning the PV panel angles to achieve the maximum power. The FLC rules are determined by observing the curve of the MPPT maximum power and the solar tracker angles. The proposed method is simulated using the Matlab-Simulink and shows the superiority in the PV energy efficiency

compared to the fixed PV panel, the conventional solar tracker, and the existing integrated solar tracker.

In the future, the proposed system will be implemented on the real hardware. Furthermore, the extended algorithm to integrate both solar tracker and MPPT methods will be investigated.

Acknowledgment. This work is supported by the Research Grant, Competence-Based Research scheme from Directorate General of Higher Education, Ministry of Research and Technology and Higher Education, Republic of Indonesia (No. 047/SP2H/LT/MULTI/L7/2019).

REFERENCES

[1] S. Racharla and K. Rajan, Solar tracking system – A review, *International Journal of Sustainable Engineering*, vol.10, no.2, pp.72-81, 2017.

[2] B. Bendib, H. Belmili and F. Krim, A survey of the most used MPPT methods: Conventional and advanced algorithms applied for photovoltaic systems, *Renewable and Sustainable Energy Reviews*, vol.45, pp.637-648, 2015.

[3] A. Díaz, R. Garrido and J. J. Soto-Bernal, A filtered sun sensor for solar tracking in HCPV and CSP systems, *IEEE Sensors Journal*, vol.19, no.3, pp.917-925, 2019.

[4] B. K. Hammad, R. H. Fouad, M. S. Ashhab, S. D. Nijmeh, M. Mohsen and A. Tamimi, Adaptive control of solar tracking system, *IET Science, Measurement & Technology*, vol.8, no.6, pp.426-431, 2014.

[5] Z. Zhen et al., The effects of inclined angle modification and diffuse radiation on the sun-tracking photovoltaic system, *IEEE Journal of Photovoltaics*, vol.7, no.5, pp.1410-1415, 2017.

[6] D. A. Flores-Hernández, S. I. Palomino-Resendiz, A. Luviano-Juárez, N. Lozada-Castillo and O. Gutiérrez-Frías, A heuristic approach for tracking error and energy consumption minimization in solar tracking systems, *IEEE Access*, vol.7, pp.52755-52768, 2019.

[7] Syafaruddin and S. Latief, A simple method for determination of electrical characteristics in different photovoltaic (PV) modules technologies, *ICIC Express Letters*, vol.12, no.9, pp.871-880, 2018.

[8] A. Chikh and A. Chandra, An optimal maximum power point tracking algorithm for PV systems with climatic parameters estimation, *IEEE Transactions on Sustainable Energy*, vol.6, no.2, pp.644-652, 2015.

[9] C. Hua, Y. Fang and C. Wong, Improved solar system with maximum power point tracking, *IET Renewable Power Generation*, vol.12, no.7, pp.806-814, 2018.

[10] A. Soetedjo, A. Lomi, Y. I. Nakhoda and A. U. Krismanto, Modeling of maximum power point tracking controller for solar power system, *TELKOMNIKA*, vol.10, no.3, pp.419-430, 2012.

[11] R. Alik and A. Jusoh, Modified Perturb and Observe (P&O) with checking algorithm under various solar irradiation, *Solar Energy*, vol.148, pp.128-139, 2017.

[12] B. A. Isaloo and P. Amiri, Improved variable step size incremental conductance MPPT method with high convergence speed for PV systems, *Journal of Engineering Science and Technology*, vol.11, no.4, pp.516-528, 2016.

[13] J. Macaulay and Z. Zhou, A fuzzy logical-based variable step size P&O MPPT algorithm for photovoltaic system, *Energies*, vol.11, no.6, pp.1-15, 2018.

[14] C. S. Chin, A. Babu and W. McBride, Design, modeling and testing of a standalone single axis active solar tracker using MATLAB/Simulink, *Renewable Energy*, vol.36, pp.3075-3090, 2011.

[15] A. Zakariah, J. J. Jamian and M. A. M. Yunus, Dual-axis solar tracking system based on fuzzy logic control and light dependent resistors as feedback path elements, *Proc. of IEEE Student Conference on Research and Development (SCOReD)*, Kuala Lumpur, Malaysia, pp.139-144, 2015.

[16] M. Haryanti, A. Halim and A. Yusuf, Development of two axis solar tracking using five photodiodes, *Proc. of Electrical Power, Electronics, Communicatons, Control and Informatics Seminar (EECCIS)*, Malang, Indonesia, pp.40-44, 2014.

[17] S. B. Elagib and N. H. Osman, Design and implementation of dual axis solar tracker based on solar maps, *Proc. of International Conference on Computing, Electrical and Electronic Engineering (ICCEEE)*, Khartoum, Sudan, pp.697-699, 2013.

[18] I. Reda and A. Andreas, Solar position algorithm for solar radiation applications, *Solar Energy*, vol.76, no.5, pp.577-589, 2004.

[19] M. E. H. Chowdhury, A. Khandakar, B. Hossain and R. Abouhasera, A low-cost closed-loop solar tracking system based on the sun position algorithm, *Journal of Sensors*, vol.2019, pp.1-11, 2019.
[20] J. J. Michalsky, The Astronomical Almanac's algorithm for approximate solar position (1950-2050), *Solar Energy*, vol.40, no.3, pp.227-235, 1988.
[21] C. Alexandru, A novel open-loop tracking strategy for photovoltaic systems, *The Scientific World Journal*, vol.2013, pp.1-12, 2013.
[22] F. I. Mustafa, A. S. Al-Ammri and F. F. Ahmad, Direct and indirect sensing two-axis solar tracking system, *Proc. of the 8th International Renewable Energy Congress (IREC)*, Amman, Jordan, pp.1-4, 2017.
[23] S. Bulárka and A. Gontean, Hybrid-loop controlled solar tracker for hybrid solar energy harvester, *Proc. of the 25th Telecommunication Forum (TELFOR)*, Belgrade, Serbia, pp.1-4, 2017.
[24] A. Halvaei Niasar, Z. Zare and F. Rabiei Far, A low-cost P&O based maximum power point tracking, combined with two-degree sun tracker, *Proc. of the 6th Power Electronics, Drive Systems & Technologies Conference (PEDSTC2015)*, Tehran, Iran, pp.119-124, 2015.
[25] H.-C. Lu and T.-L. Shih, Fuzzy system control design with application to solar panel active dual-axis Sun tracker system, *Proc. of IEEE International Conference on Systems, Man and Cybernetics*, Istanbul, Turkey, pp.1878-1883, 2010.
[26] H. Fathabadi, Novel online sensorless dual-axis Sun tracker, *IEEE/ASME Transactions on Mechatronics*, vol.22, no.1, pp.321-328, 2017.
[27] M. Blanco-Muriel, D. C. Alarcon-Padilla, T. Lopea-Moratalla and M. Lara-Coira, Computing the solar vector, *Solar Energy*, vol.70, no.5, pp.431-441, 2001.
[28] Z. Jagoo, *Tracking Solar Concentrators – A Low Budget Solution*, Springer, Heidelberg, 2013.
[29] *http://stjarnhimlen.se/comp/tutorial.html#5*, 2019.
[30] *http://www.stargazing.net/kepler/altaz.html*, 2019.
[31] *https://www.mathworks.com/matlabcentral/fileexchange/23051-vectorized-solar-azimuth-and-elevation-estimation*, 2019.
[32] K. Boudaraia, H. Mahmoudi, M. Abbou and M. Hilal, DC motor position control of a solar tracking system using second order sliding mode, *Proc. of the 5th International Conference on Multimedia Computing and Systems (ICMCS)*, Marrakech, Morocco, pp.594-598, 2016.
[33] G. R. Walker, Evaluating MPPT converter topologies using a MATLAB PV model, *Journal of Electrical & Electronics Engineering*, vol.21, no.1, pp.49-56, 2001.
[34] *http://ecee.colorado.edu/∼ecen5797/course_material/SimulinkSlides.pdf*, 2019.
[35] *https://www.mathworks.com/help/physmod/sps/examples/stepper-motor-with-control.html*, 2019.